Feasibility of Insect Identification Based on Spectral Fringes Produced by Clear Wings

Meng Li, Anna Runemark, Noélie Guilcher, Julio Hernandez, Jadranka Rota, and Mikkel Brydegaard

***Abstract*—Due to the growing awareness that insects' diversity and populations are in decline, there is an increased need for monitoring insects. Entomological lidars and photonic sensors can monitor and remotely identify flying insects based on their backscattered signal in terms of oscillations-, polarization-, and spectral content. The backscattered light from insects is predominantly oscillatory and derives from the wings. This part of the signal is also more coherent and co-polarized than the light reflected from the insect's abdomen. Clear membranes can display soap-bubble colors due to thin-film interference, a feature that can be associated with the thickness of the wing. A hyperspectral camera can capture these wing interference patterns with hundreds of spectral bands and accurately identify the wing thickness. Here we investigate whether the spectral fringes can provide complementary information to aid remote species identification. We demonstrate that we can extract wing thickness and modulation depth information from spectral fringes of 87 species of common insect pollinators in Skåne, Sweden. The modulation depth of a fringe provides information related to insect wing thickness homogeneity, wrinkledness, or anti-reflectance features. Our results show that examined species display distinct modulation and wing thickness, and therefore such features can be used to improve the specificity of species identification of photonics sensors.**

***Index Terms*—Spectral fringe, insect, pollinator, entomological lidar, wing thickness, hyperspectral, thin-film.**

I. Introduction

INSECT habitats and populations are adversely affected by human-driven disturbances and global warming [1], [2], [3]. Despite the fact that insects have high resilience and an incredible capacity to reproduce, there has been a decline in insect populations [4] and diversity [5], [6] over the years. Insects are essential to our ecosystems [7]. They are a key part of the food chain and play an important role in pollination. They also help to control pests and can be used as indicators of environmental health. The decrease in diversity and population of pollinators has negative effects on ecosystem functioning [8] and agricultural production [9]. To protect and manage wild pollinators, it is crucial to be able to monitor insects' diversity and distribution. Additionally, monitoring will enable predicting changes in insect population sizes in response to management strategies for the landscape [10], [11].

However, it remains a challenge to monitor insects using conventional catch-based survey methods. Adult insects, which are usually the main target for monitoring [12], [13], [14], are only present for a short period of time and appear at a specific time of the day and year. Consequently, insects captured with conventional catch-based methods come with strong biases [15]. Baits or pheromones used in traps are also generally designed to attract certain species. Methods based on catching and identifying species of insects are also very labor-intensive and require an experienced taxonomist. Genetic methods have recently been used to identify trapped insect species, but they could not report values in insect abundance [16].

Compared to conventional trap-based methods, laser remote sensing [17], [18] can provide unbiased data on insect activity and flux in situ with very high spatial and temporal resolution [19]. Such information could be used to monitor pests [20], track the spread of disease vectors [21], and monitor and manage agricultural pests or pollinators [22]. Machine vision and imaging-based techniques have been reported in combination with traps [23], [24], but focusing challenges imply that recognition of anatomical details is difficult for free-flying insects [25]. Fortunately, methods based on wing beat oscillation-, polarization- and spectral- features of the insects can retrieve signals regardless of focus on insects appearing sparsely in time and space [17], [21].

Insect species have distinct wing beat frequencies and distinct compositions of overtones. These signals have been demonstrated to enable species discrimination in flight chambers [26], [27], and multiple groups of insects have been differentiated in the field based on their oscillatory properties [10], [28].

In complement to oscillation signatures of detected insects, we explore if multiple polarization- or spectral bands could increase the number of discernable species. Detailed spectral information from insect bodies can be used to differentiate insect species, sex, and age [29], [30]. Oscillatory signals from free-flying insects can be expanded to discriminate co- and

Manuscript received 26 August 2022; revised 6 October 2022; accepted 27 October 2022. Date of publication 31 October 2022; date of current version 10 November 2022. This work was supported by the European Research Council under through the European Union's Horizon 2020 Research and Innovation Programme under Grant 850463. *(Corresponding author: Meng Li.)*

Meng Li and Anna Runemark are with the Department of Physics and Department of Biology, Lund University, 22363 Lund, Skåne, Sweden (e-mail: meng.li@forbrf.lth.se; anna.runemark@biol.lu.se).

Noélie Guilcher is with the Department of Biology, Polytech Clermont Ferrand 63170 Aubiére, France (e-mail: noelie.guilcher@gmail.com).

Julio Hernandez is with the Norsk Elektro Optikk A/S, Norway (e-mail: julio@neo.no).

Jadranka Rota is with the Biological Museum, Department of Biology, Lund University, 22362 Lund, Skåne, Sweden (e-mail: jadranka.rota@biol.lu.se).

Mikkel Brydegaard is with the Department of Physics and Department of Biology, Lund University, 22363 Lund, Skåne, Sweden, and also with Norsk Elektro Optikk A/S 0667 Oslo, Norway (e-mail: mikkel.brydegaard@fysik.lth.se).

Color versions of one or more figures in this article are available at https://doi.org/10.1109/JSTQE.2022.3218218.

Digital Object Identifier 10.1109/JSTQE.2022.3218218

de-polarized backscatter both in caged environments [20], [26], [27] and in situ [31]. This allows for the discrimination of coherent specular and incoherent diffuse scattering. If the wavelength resonates with the wing membrane thickness, rapid specular flashes appear on the scattered waveform, and consequently, a large number of harmonics appear. Both polarized recordings with photonic sensor environments on insects in cages [20], [26], [27] and lidar field recordings [31] show that most of the scattered signals from insects is oscillatory and specular, and WIPs account for most of the optical signature ($\sim$80%) of free-flying clear winged insects [31]. Flat clear wings of insects can exhibit reflectance 50 times more than a diffuse white at the resonant wavelength [31]. This is far brighter than any diffuse light reflected from vegetation or the sky background. Insect sensors [18], [19], [32] or lidars [20], [31], [33] with dual- or multiple wavelength bands are, therefore highly sensitive to Wing Interference Patterns (WIPs) and could potentially distinguish species based on wing thickness. Like some polarimetric insect vision systems, polarimetric lidars can also further enhance contrast for resonant backscatter from WIPs against the natural environment [31].

For clear-winged insect pollinators, a dominant spectral feature is thus the spectral fringe produced from their thin wing membrane associated with the wing thickness, also known as WIPs. This feature is stable over time and generations, according to studies on museum specimens [34]. Studies on WIPs suggest that the variation is low within species but high among species [35], [36]; thus, wing thickness could be the ideal parameter for discerning species.

Morphological data of insects could improve the interpretation of oscillatory signals [37], whereas differences in nano- and micro-surface structures could improve specificity in multispectral systems [38]. Allometric relationships between insect size and the morphology of their wings are known for a range of species [39], [40], [41], and allometric relationships are typically hard to alter. However, the relationship between wing area and wing thickness is not well studied. It is interesting to study allometry to understand how insects make morphological changes in order to maintain the same performance despite their size differences and whether wing thickness scales allometrically with wing size for biomechanical reasons or if it is locked by species interactions or sexual selection.

In this study, we investigated if spectral fringes could provide information complementary to improving remote insect identification in optical sensing. Specifically, we captured the spectral fringes and measured the wing thickness of 87 species belonging to the most important groups of distinct insect pollinators: bees, wasps, and flies. The aim was to examine the feasibility of using fringe information to improve the remote identification of more species with lidar or other optical techniques by recording both wing-beat modulation and spectral information simultaneously.

II. Materials and Methods

The Lund University Biological Museum provided 87 species of pollinators representing 8 families from two insect orders (Hymenoptera and Diptera) with 1 specimen of each. These species of bees, wasps, and flies were selected as they are important pollinators and are difficult to identify for amateurs. They also have clear and flat wings, increasing the feasibility of using spectral fringes for identification. The species included in this study are presented in Table I.

The experimental setup is shown in Fig. 1. A hyperspectral camera with 288 spectral bands from 0.95 μm to 2.5 μm was used to capture the spectral fringes from the wings [42]. Melanin contribution from the wings can be neglected in this wavelength region. A 150 W broadband halogen lamp was used to illuminate the wings, and two ultra-broadband polarizers [43] were used to capture co- and de-polarized reflectance. The angle of incidence and observation were $\pm 56^{\circ}$. The objective of the camera had an aperture of Ø20 mm, and a working distance of 30 cm (forming a light cone of 3.8°). Mirrored spheres were used to image the size and position of the light source [44], [45]; the reflection of the light source on the spheres provides information on the convolution of the light cone from the source (15°) and cone received by the camera. All hyperspectral data were calibrated to a diffused grey reflectance standard with 50% reflectance (Spectralon); a specular pixel calibrated to such a diffused standard will exceed 100% diffuse reflectance. All samples were mounted on black neoprene with horizontal wing surfaces. Black neoprene was used to reduce the background light. One wing of each specimen was scanned, and sexual dimorphism was not taken into consideration in this study. We only scanned one wing because most specimens did not have both their wings spread, as it is not a common procedure in preparing and storing specimens of Hymenoptera and Diptera orders of insect specimens.

III. Results

When a clear insect wing is illuminated by a white light source, different wavelengths of light are attenuated or resonant depending on the membrane thickness, which results in the soap bubble color patterns appearing on the wing that are visible in both RGB and false-color images shown in Fig. 2(a), (b). The red and blue arrows in Fig. 2(b), (c) illustrate the incident- and captured ray paths and polarizations. Dots on the red and blue arrows in Fig. 2(b) indicate that incident and capture light are both horizontally polarized, whereby an co-polarized image is acquired. The dots and smaller arrows on the red and blue arrows in Fig. 2(c) show the incident light is horizontally polarized, and the captured light is vertically polarized, as the polarization directions are perpendicular, the signal captured by the camera is de-polarized. Specular pixels from the wings are only present in the co-polarized false-color image shown in Fig. 2(b), not in the de-polarized image shown in Fig. 2(c), which indicates the light reflected from the wing membrane is a coherent phenomena.

As different wavelengths either resonate in forward- or backscattering depending on the wing thickness, the spectral profile of each wing pixel display a spectral fringe [46]. Examples of a thicker and a thinner wing pixel highlighted by two arrows in Fig. 2(b) have corresponding spectral fringes shown in Fig. 2(d). The effective fringe shown in Fig. 2(d) of the entire wing acquired by spatially averaging all wing pixels. Wing thickness is calculated for all 3 fringes shown in Fig. 2(d) by a

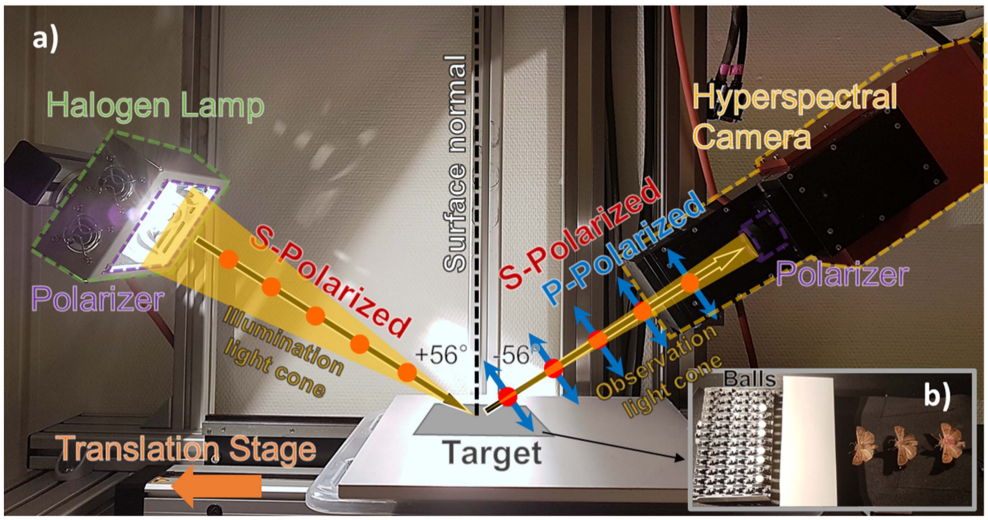

Fig. 1. (a) The experimental configuration used for hyperspectral imaging. The illuminator was equipped with a large wire grid polarizer, and another linear polarizer was placed in front of the camera. This analyzer can be rotated to alternate between capturing co- and de-polarized reflectance. (b) The order of objects included in each scan were: Chrome spheres, teflon spheres, a flat grey diffuse standard, and insects mounted on black neoprene.

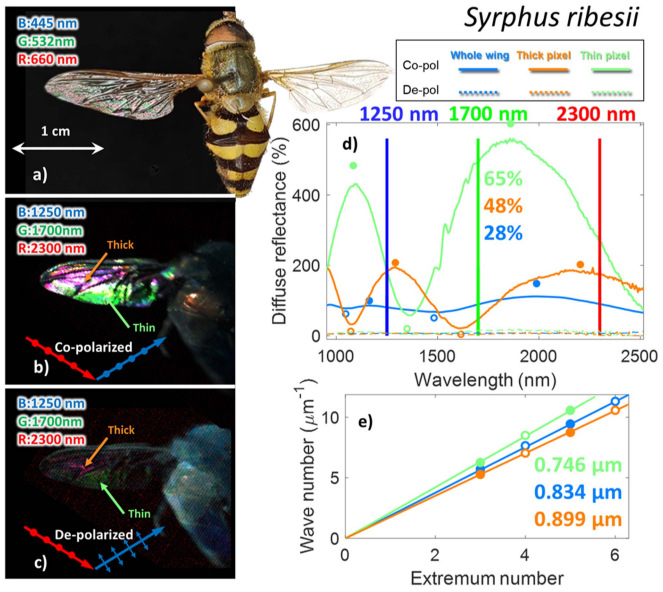

Fig. 2. (a) Soap bubble colors on the wing are more visible when the insect wing is placed against a black background. (b-c) Two false-color images were generated for co- and de-polarizations. The orange and green circles in (b-c) correspond to two wing pixels from a thicker and thinner region of the wing; Blue colored reflectance spectrum in (d) corresponds to the effective wing reflectance integrated over the whole wing. Value 28, 48, and 65% describe how modulated its corresponding fringe. (e) Reflectance maxima are illustrated with closed circles, and minima are illustrated with open circles from (d).

linear fitting method with extremum numbers (Fig. 2(e)) [46]. The two selected pixels in Fig. 2(b), (c) with different thicknesses display different colors (thicker: pink, thinner: green, in this particular false color visualization); the thin pixel fringe has a larger modulation depth than thick pixel (see Fig. 2(d)), and the thick fringe is more fringed than the thin fringe in the spectral window. Modulation depth (M) measures how pronounced the fringe effect is for a given wing. If modulation depth approach zero, the accuracy of wing thickness estimation would vanish. The mean- and standard deviation of reflectance are considered in the spectral domain. The modulation depth is expressed as:

$$M = \frac{\sigma(R_\lambda) \cdot \mu(F_\lambda)}{\sigma(F_\lambda) \cdot \mu(R_\lambda)} \tag{1}$$

where R is measured reflectance and F is computed fringe, λ is the wavelength, σ is the standard deviation, and μ is the mean of the sample. Based on the Fresnel equation and thin-film physics, its reflectance fringe $F(\lambda)$ can be expressed as [47],

$$F(\lambda, d) = \frac{4R_s \sin^2\left(2\pi d\sqrt{n^2 - \sin^2\theta}/\lambda\right)}{(1 - R_s)^2 + 4R_s \sin^2\left(2\pi d\sqrt{n^2 - \sin^2\theta}/\lambda\right)} \tag{2}$$

where n is the refractive index of the chitin, d is the thickness of the wing, θ is the incident angle to the wing membrane, λ is the wavelength, and r is the reflection coefficient by Fresnel equations. The refractive index of the cuticle is expressed as [46]:

$$n = k_0 + k_1/\lambda^2 \tag{3}$$

where $k_0 = 1.517$ and $k_1 = 8800$ nm^2. For S-polarization (electric field is perpendicular to the plane of incidence), the reflection coefficient R_s is expressed as:

$$R_s = \left(\frac{\cos\theta - \sqrt{n^2 - \sin^2\theta}}{\cos\theta + \sqrt{n^2 - \sin^2\theta}}\right)^2 \tag{4}$$

The reflectance from P-polarization should be absent in our case since we measure at the Brewster angle. The crossed de-polarized P-polarized signal thus only captures multiple scattered lights from veins; as can be seen in Fig. 2(c), (d) this contribution is minimal compared to the fringed coherent reflectance. Thus fringes are horizontally co-polarized (S-polarization) as

TABLE I
LIST OF THE 87 SPECIES OF INSECT POLLINATORS STUDIED

Family	Genus	Specie	d_{eff} (μm)	M (%)	A (mm^2)
Andrenidae	*Andrena*	*barbilabris*	0.95	36	28.4
		carantonica	1.23	21	32.2
Apidae	*Bombus*	*cineraria*	1.49	14	31.2
		clarkella	1.00	22	39.0
		denticulata	1.10	24	15.9
		flavipes	0.94	15	18.9
		fucata	1.13	23	19.3
		fulva	0.74	27	28.8
		fuscipes	1.05	21	15.8
		haemorrhoa	0.82	22	24.9
		hattorfiana	1.02	17	37.4
		helvola	0.66	31	30.4
		lapponica	1.10	16	12.7
		lathyri	1.30	17	24.7
		minutula	0.49	47	8.69
		nigroaenea	0.74	20	25.7
		praecox	0.79	38	24.7
		ruficrus	0.39	49	12.4
		semilaevis	0.57	22	9.57
		subopaca	0.45	45	10.8
		tibialis	1.21	18	51.0
		vaga panzer	1.43	28	32.3
		wilkella	0.79	32	18.5
	Apis	*mellifera*	1.07	14	28.9
	Bombus	*bicornis*	0.98	20	17.8
		bohemicus	1.86	11	68.3
		campestris	1.98	10	45.7
		distinguendus	2.33	12	55.9
		hortorum	1.79	12	69.6
		humilis	2.67	11	51.6
		hypnorum	1.24	11	38.7
		jonellus	0.94	16	20.7
		lapidarius	2.49	9	81.2
		magnus	1.86	9	66.9
		muscorum	2.31	8	81.3
		pascuorum	1.54	9	49.1
		pratorum	2.29	15	50.8
		ruderarius	2.35	11	51.5
		rupestris	3.79	18	117
		soroeensis	2.63	14	69.9
		sporadicus	1.28	11	78.8
		terrestris	2.37	10	51.7
		veteranus	1.32	6	51.0
Colletidae	*Hylaeus*	*annulatus*	0.69	10	6.65
		brevicornis	0.73	18	6.36
		communis	1.42	11	7.09
		confusus	1.02	41	6.86
		gibbus	0.50	37	10.0
		hyalinatus	0.62	35	5.01
Halictidae	*Lasioglossum*	*fulvicorne*	0.49	36	9.99
		leucopus	0.41	17	6.31
		morio	0.48	25	12.8
		quadrinotatum	0.60	56	10.9
		sexstrigatum	0.51	35	3.04
		villosulum	0.82	22	10.4
Megachilidae	*Megachile*	*centuncularis*	1.16	14	21.6
		circumcincta	1.56	20	32.0
		lagopoda	1.99	17	39.2
		lapponica	1.14	18	15.9
		versicolor	1.25	16	22.2
		willughbiella	1.44	16	25.9
	Osmia	*caerulescens*	1.34	13	10.3
		leaiana	0.96	24	12.5
Syrphidae	*Episyrphus*	*balteatus*	0.94	12	19.3
	Eupeodes	*corollae*	0.81	18	22.7
	Melanostoma	*mellinum*	0.52	39	12.0
	Scaeva	*pyrastri*	1.17	15	49.1
	Sphaerophoria	*scripta*	0.57	41	11.4
	Syrphus	*ribesii*	0.85	30	15.8
		vitripennis	0.87	18	27.3
Tabanidae	*Tabanus*	*bovinus*	1.13	7	98.8
Vespidae	*Ancistrocerus*	*claripennis*	0.93	31	16.7
		nigricornis	1.07	15	25.8
		oviventris	1.39	16	17.4
		parietinus	1.08	18	26.8
		parietum	0.75	15	26.1
		trifasciatus	1.02	18	31.8
	Dolichovespula	*saxonica*	1.61	16	48.5
	Eumenes	*coronatus*	1.19	18	28.3
		notatus	1.09	20	17.9
	Odynerus	*spinipes*	1.45	20	25.9
	Symmorphus	*allobrogus*	0.83	29	13.1
		bifasciatus	0.35	26	9.08
	Vespa	*crabro*	2.18	18	65.4
	Vespula	*germanica*	1.20	23	32.7
		rufa	1.44	15	59.0
		vulgaris	1.42	16	47.2

shown in Fig. 2(b), (c), (d); therefore, only reflection coefficient r_s was used in developing the fringe model in (2).

The modulation depth was calculated for 3 example fringes shown in Fig. 2(d) with their values shown in the same plot; the effective fringe (whole wing) has the lowest modulation, and it is attenuated towards the shorter wavelengths. To investigate the reasons for the decrease in the modulation depth of the effective fringe compared to individual specular wing pixels (for example, thick and thin fringes), the wing thickness and modulation depth were calculated and documented for all wing pixels for the same wing shown in Fig. 2(b) and in Table I. Instead of the peak-valley fitting in Fig. 2(e) [46], the fringe model $F(\lambda)$ in (2) was used to determine wing thickness for all wing pixels. Fringe model $F(\lambda,d)$ was first used to generate multiple (1000) computed fringes with wing thicknesses 0.35 μm$<d<4$ μm, the modulation of $F(\lambda,d)$ is always 100% because it lacks bias terms. Each computed fringe $F(\lambda,d)$ was then compared to the measured fringe $R(\lambda)$ from a wing pixel, according to the correlation, C, in (5). We then introduced a fit quality parameter, Q in (6):

$$C\ (R, F(d)) = \frac{\int_{0.35}^{4} \left(F_{\lambda,d} - \mu\left(F_{\lambda,d}\right)\right)\left(R_{\lambda} - \mu\left(R_{\lambda}\right)\right)}{\sqrt[2]{\int_{0.35}^{4} \left(F_{\lambda,d} - \mu\left(F_{\lambda,d}\right)\right)^2 \partial\lambda \int_{0.35}^{4} \left(R_{\lambda} - \mu\left(R_{\lambda}\right)\right)^2 \partial\lambda}} \tag{5}$$

$$Q(d) = C(R,F)\left(C\left(\frac{\partial R}{\partial \lambda}, \frac{\partial F}{\partial \lambda}\right)\right)^2 \tag{6}$$

Here the spectral derivatives are used to ignore slope differences. The squared power is needed to avoid double negative correlation coefficients.

Wing thickness and modulation of all wing pixels from the example wing shown in Fig. 2 were estimated and presented as a wing thickness map, and a wing modulation depth map in Fig. 3(a). The wing thickness map example shows that wings are generally thicker around the frontal edges (costal margin) and thinner near the rear edge (anal margin). It is important to note that the membrane thickness in Fig. 3 is based on the thin film principle and does not describe vein thicknesses. However, vein pixels also have very low modulation depth, as shown in Fig. 3(a), and their influence on the effective fringe is relatively small.

The density plot of thicknesses and modulation in Fig. 3(b) shows that there is a large variation in wing thickness across the wing. The thickness histogram reveals specific thickness preferences; for example, thickness at 1.0 μm and 1.2 μm is more dominant than wing thickness at 1.1 μm. A relevant question is if these nanoscale thicknesses are quantized. Studies of chitin polymers in lobster's exoskeletons [48] displayed specific folding and curling preferences of the chitin polymer.

The density plot in Fig. 3(b) also shows that the fringes of a large amount of wing pixels display high modulation depths. The fringes with high modulation also correspond to specific prominent wing thicknesses (see Fig. 3(a)). Thicker wing pixels produce narrow spectral fringes than thin wing pixels. Thus,

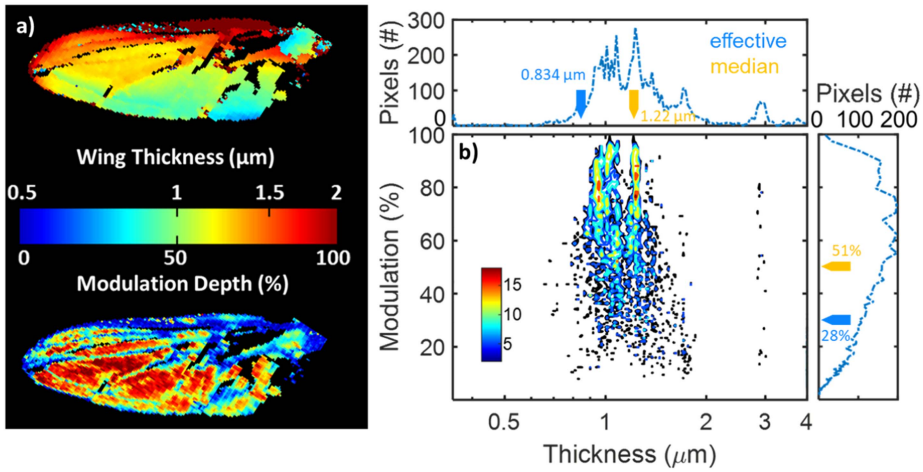

Fig. 3. (a) Wing thickness and modulation depth maps of the same example wing shown in Fig. 2. (b) Wing thickness and modulation distribution and histograms. Yellow arrows indicate the location of medians in both wing thickness and modulation. Blue arrows indicate the position of effective wing thickness and modulation calculated and presented in Fig. 2. The effective fringe modulation is lower than the median of all fringes.

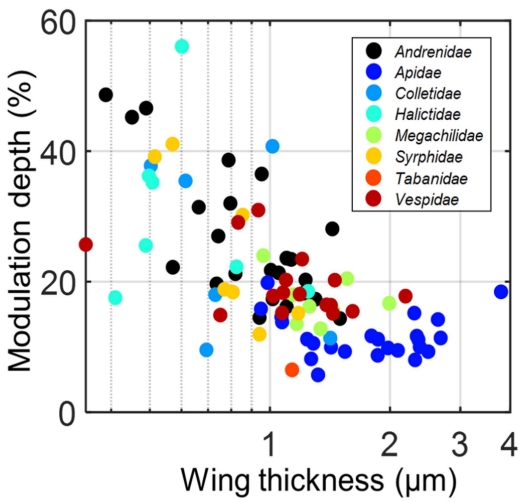

Fig. 4. Effective wing thickness and modulation depth were investigated for a large selection of insect species while each family of insects is color-coded.

fringes across the wing surface are more likely to interfere constructively with thin wings and for long wavelengths. Examples where fringe resonance modes are out of phase are shown in Fig. 2(d) with thick and thin fringes. Consequently, the effective modulation is reduced.

The effective wing thickness, d_{eff}, and modulation were then estimated for 87 species of Hymenoptera (bees and wasps) and Diptera (mainly hover flies), see Table I. This estimation was based on the effective fringe from their entire wings (the effective fringe for *S. ribesii* is shown in Fig. 2(d). All 87 studied individuals were museum specimens, each representing a different species, belonging to 8 different families. The effective modulation depth was investigated for all specimens and color-coded at the family level (not spread of individual species). Note that modulation values are valid only for the spectral window of our instrument. In Fig. 4, it can be seen that the insect family Apidae, which includes, for example, honeybees and bumblebees, and the family Megachilidae, which includes mason bees and leafcutter bees, display a wide variation in wing thickness and low modulation. We find that Vespidae, the family comprising wasps, has a wide wing thickness distribution and a medium degree of modulation depth among all studied species. Only one specimen of Tabanidae, a horsefly, was investigated, and it displayed a low degree of modulation depth. The rest of the insect families display a high degree of modulation depth.

All scatter points in Fig. 4 show a trend that thin wings display higher modulation depths; this could be explained by three reasons: 1) the modulation could be damped due to wrinkled wings, 2) nanostructures on some wings can induce anti reflectance effect by gradient refractive index interfaces [46], 3) fringes from a thicker wing are narrow in the spectral domain, thus more likely to get out of phase due to thickness heterogeneity causing the reduction in modulation depth, whereas fringes from a thin wing are less sensitive to phase displacement. This can also explain why the effective fringe modulation is getting higher in the longer wavelengths (see Fig. 2(d) effective fringe). We found the last explanation most plausible.

The relation between wing thickness and wing area was investigated for all species and presented in Fig. 5. A squared power relation of wing area, A (mm^2), and effective wing thickness $d_{eff.}$ (μm) indicate allometric scaling, which is illustrated with a grey line in Fig. 5, with a scaling factor of 17 [16–19, confidence interval]. However, the relationship is better described by the relation colored in red, with a scaling factor of 23 [21–26, confidence interval] and a power relation of 1.2 [1.0–1.3] instead of squared. The result in Fig. 5 shows there is a 74% $R^2_{\mathrm{adj.}}$ correlation between wing area and wing thickness (described by the power relation), the correlation described by the squared relation is only 41% $R^2_{\mathrm{adj.}}$; the thickness is not scaling allometrically with wing area. Moreover, the power relation seemingly fails to describe all families; for example, the family Colletidae displays a range of thicknesses with a negligible change in wing areas. This means the scaling relation between wing area and thickness could be family specific, and despite the correlation area alone could not

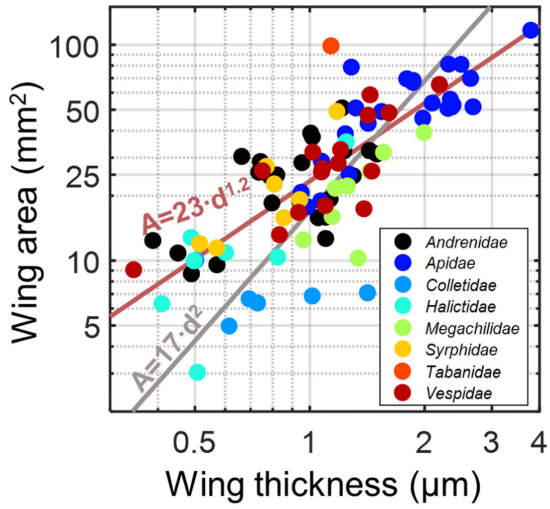

Fig. 5. Effective wing thickness and wing area relation was investigated, they show a strong correlation.

explain thickness variations. This encourages improved specificity by acquiring fringes.

IV. Discussion

Our results suggest that the wing thickness of these groups of pollinators ranges from ∼0.5 to 2 μm. We found that some insect families do produce strong modulated effective fringes even when the signals from the whole wings are integrated, in particular when the wing membrane is thin. This effect could yield complementary information in addition to wing beat modulation, or it could be used to employ strategically resonant wavelengths in order to improve detection range or signal-to-noise. We also found that pixel modulation depth for examined insects is always lower than 100%, which implies that accurate thickness assessment is not possible by Newton rings color-coding and RGB imaging in previous studies (computer generated newton series scale of two-beam interference colors), thus multi- or hyperspectral methods are needed.

For many species of Apidae, especially species of bumblebees (genus *Bombus*), the wing segments are not in a single plane and display a large thickness variation across the wings, and this attenuates modulation depth. The species in the families Andrenidae (e.g., ground-nesting bees), Colletidae (e.g., plasterer bees), Halictidae (e.g., sweat bees), and Syrphidae (e.g., hover flies) displayed high modulation depth. Insect species with thin wings (∼0.5 to 1 μm) will have a higher potential to be detected from a long distance with its relatively high modulation depth, as fringes of thin membranes are also less sensitive to the damping of modulation due to the resonance modes getting out of phase. Effective fringes also become broader at longer wavelength regions and become hard to get out of phase, resulting in an increase in the effective modulation depth. This motivates infrared methods to capture this effect. The wing thickness strongly (74% R^2_{ajd}) correlated to wing area, but such relation scaling can differ between families.

During this initial survey, we only measured 1 specimen of each species, and we did not study the sexual dimorphism among species. WIPs play a role in the mating choice for some species [36], [49], [50]. Hence, sexual selection based on WIPs might prevent wing thickness from scaling allometrically with wing size. In the future, we will assess within-species variation by measuring multiple specimens of each species, sex, and distinct size. Despite our small sample size, we have provided realistic expectations of the thickness and effective modulation of examined 87 species of insect pollinators. Effective wing thickness, together with the fringe model, provide essential information to assist the development of photonics sensors; by placing sensors' laser band at the resonant wavelength of WIPs to maximize the retrieved signal magnitude and contrast for targeted insect specie. Our data will prove crucial for designing optical sensors for insect monitoring. Distinctness of wing thickness and modulation between insect families opens up the possibility for remote species identification using WIPs.

Acknowledgment

We gratefully acknowledge the fruitful discussion and comments from Benjamin Thomas.

Materials & Correspondence

Correspondence and requests for materials should be addressed to ML.

References

[1] A. Holzschuh, I. Steffan-Dewenter, and T. Tscharntke, "How do landscape composition and configuration, organic farming and fallow strips affect the diversity of bees, wasps and their parasitoids?," *J. Animal Ecol.*, vol. 79, no. 2, pp. 491–500, 2010.

[2] C. Robinet and A. Roques, "Direct impacts of recent climate warming on insect populations," *Integrative Zoology*, vol. 5, pp. 132–142, Jun. 2010.

[3] T. Tscharntke et al., "Insect conservation in agricultural landscapes," *Insect Conservation Biol.*, vol. 16, pp. 383–404, 2007.

[4] C. A. Hallmann et al., "More than 75 percent decline over 27 years in total flying insect biomass in protected areas," *PLoS One*, vol. 12, no. 10, 2017, Art. no. e0185809.

[5] M. L. Forister, E. M. Pelton, and S. H. Black, "Declines in insect abundance and diversity: We know enough to act now," *Conservation Sci. Pract.*, vol. 1, no. 8, 2019, Art. no. e80.

[6] R. van Klink et al., "Meta-analysis reveals declines in terrestrial but increases in freshwater insect abundances," *Science*, vol. 368, no. 6489, pp. 417–420, 2020.

[7] J. C. Miller, "Insect natural history, multi-species interactions and biodiversity in ecosystems," *Biodiversity Conservation*, vol. 2, no. 3, pp. 233–241, 1993.

[8] B. J. Brosi and H. M. Briggs, "Single pollinator species losses reduce floral fidelity and plant reproductive function," *Proc. Nat. Acad. Sci.*, vol. 110, no. 32, pp. 13044–13048, 2013.

[9] M. A. Aizen and L. D. Harder, "The global stock of domesticated honey bees is growing slower than agricultural demand for pollination," *Curr. Biol.*, vol. 19, no. 11, pp. 915–918, Jun. 2009.

[10] M. Brydegaard et al., "Lidar reveals activity anomaly of malaria vectors during pan-African eclipse," *Sci. Adv.*, vol. 6, no. 20, May 2020, Art. no. eaay5487.

[11] N. M. A. El-Ghany, S. E. A. El-Aziz, and S. S. Marei, "A review: Application of remote sensing as a promising strategy for insect pests and diseases management," *Environ. Sci. Pollut. Res.*, vol. 27, no. 27, pp. 33503–33515, Sep. 2020.

[12] D. L. Kline, "Traps and trapping techniques for adult mosquito control," *J. Amer. Mosquito Control Assoc.*, vol. 22, no. 3, pp. 490–496, 2006.

[13] E. M. Raebel, T. Merckx, P. Riordan, D. W. Macdonald, and D. J. Thompson, "The dragonfly delusion: Why it is essential to sample exuviae to avoid biased surveys," *J. Insect Conservation*, vol. 14, no. 5, pp. 523–533, Oct. 2010.

[14] S. D. Wratten, A. J. White, M. H. Bowie, N. A. Berry, and U. Weigmann, "Phenology and ecology of hoverflies (Diptera: Syrphidae) in New Zealand," *Environ. Entomology*, vol. 24, no. 3, pp. 595–600, 1995.
[15] R. Muirhead-Thompson, "Trap responses of flying insects: The influence of trap design on capture efficiency," *Bull. Entomological Res.*, vol. 82, no. 3, pp. 433–434, Sep. 1992.
[16] R. Meier, W. Wong, A. Srivathsan, and M. Foo, "$1 DNA barcodes for reconstructing complex phenomes and finding rare species in specimen-rich samples," *Cladistics*, vol. 32, no. 1, pp. 100–110, 2016.
[17] M. Brydegaard and S. Svanberg, "Photonic monitoring of atmospheric and aquatic fauna," *Laser Photon. Rev.*, vol. 12, no. 12, 2018, Art. no. 1800135.
[18] K. Rydhmer et al., "Automating insect monitoring using unsupervised near-infrared sensors," *Sci. Rep.*, vol. 12, no. 1, pp. 1–11, 2022.
[19] A. Genoud, G. Williams, and B. Thomas, "Continuous monitoring of aerial density and circadian rhythms of flying insects in a semi-urban environment," *PLoS One*, vol. 16, Nov. 2021, Art. no. e0260167.
[20] M. Li et al., "Bark beetles as lidar targets and prospects of photonic surveillance," *J. Biophotonics*, vol. 14, no. 4, 2020, Art. no. e202000420.
[21] S. Jansson et al., "Real-time dispersal of malaria vectors in rural Africa monitored with lidar," *PLoS One*, vol. 16, no. 3, 2021, Art. no. e0247803.
[22] K. Rydhmer et al., "Scheimpflug lidar range profiling of bee activity patterns and spatial distributions," *Animal Biotelemetry*, vol. 10, no. 1, pp. 14–27, Apr. 2022.
[23] K. Bjerge et al., "An automated light trap to monitor moths (Lepidoptera) using computer vision-based tracking and deep learning," *BioRxiv*, 2020, Art. no. 2020.03.18.996447.
[24] L. Wührl et al., "DiversityScanner: Robotic handling of small invertebrates with machine learning methods," *Mol. Ecol. Resour.*, vol. 22, no. 4, pp. 1626–1638, 2022.
[25] S. Butail et al., "Reconstructing the flight kinematics of swarming and mating in wild mosquitoes," *J. Roy. Soc. Interface*, vol. 9, no. 75, pp. 2624–2638, 2012.
[26] A. Gebru et al., "Multiband modulation spectroscopy for determination of sex and species of mosquitoes in flight," *J. Biophotonics*, vol. 11, no. 8, 2018, Art. no. e201800014.
[27] A. Genoud, Y. Gao, G. Williams, and B. Thomas, "Identification of gravid mosquitoes from changes in spectral and polarimetric backscatter cross-sections," *J. Biophotonics*, vol. 12, Jun. 2019, Art. no. e201900123.
[28] B. K. Kouakou, S. Jansson, M. Brydegaard, and J. T. Zoueu, "Entomological scheimpflug lidar for estimating unique insect classes in-situ field test from Ivory Coast," *OSA Continuum*, vol. 3, no. 9, pp. 2362–2371, Jul. 2020.
[29] M. T. Sikulu, "Non-destructive near infrared spectroscopy for simultaneous prediction of age and species of two major African malaria vectors: An. gambiae and an. arabiensis," *NIR News*, vol. 25, no. 5, pp. 4–6, 2014.
[30] M. T. Sikulu-Lord et al., "Near-infrared spectroscopy, a rapid method for predicting the age of male and female wild-type and Wolbachia infected Aedes aegypti," *PLoS Neglected Trop. Dis.*, vol. 10, no. 10, 2016, Art. no. e0005040.
[31] M. Brydegaard, S. Jansson, M. Schulz, and A. Runemark, "Can the narrow red bands of dragonflies be used to perceive wing interference patterns?," *Ecol. Evol.*, vol. 8, no. 11, pp. 5369–5384, 2018.
[32] A. Gebru, M. Brydegaard, E. Rohwer, and P. Neethling, "Probing insect backscatter cross-section and melanization using kHz optical remote detection system," *J. Appl. Remote Sens.*, vol. 9975, pp. 23–39, 2016.
[33] M. Brydegaard and S. Jansson, "Advances in entomological laser radar," *J. Eng.*, vol. 2019, no. 21, pp. 7542–7545, 2019.
[34] E. Shevtsova, C. Hansson, D. H. Janzen, and J. Kjaerandsen, "Stable structural color patterns displayed on transparent insect wings," *Proc. Nat. Acad. Sci.*, vol. 108, no. 2, pp. 668–673, Jan. 2011.
[35] E. Shevtsova and C. Hansson, "Species recognition through wing interference patterns (WIPs) in Achrysocharoides Girault (Hymenoptera, Eulophidae) including two new species," *Zookeys*, vol. 2011, no. 154, pp. 9–30, 2011.
[36] N. J. Butterworth, T. E. White, P. G. Byrne, and J. F. Wallman, "Love at first flight: Wing interference patterns are species-specific and sexually dimorphic in blowflies (Diptera: Calliphoridae)," *J. Evol. Biol.*, vol. 34, no. 3, pp. 558–570, 2021.
[37] C. Kirkeby, M. Wellenreuther, and M. Brydegaard, "Observations of movement dynamics of flying insects using high resolution lidar," *Sci. Rep.*, vol. 6, no. 1, pp. 1–11, 2016.
[38] M. Li et al., "Potential for identification of wild night-flying moths by remote infrared microscopy," *Roy. Soc. Interface*, vol. 19, no. 191, 2022, Art. no. 20220256.
[39] R. Sacchi and S. Hardersen, "Wing length allometry in Odonata: Differences between families in relation to migratory behaviour," *Zoomorphology*, vol. 132, no. 1, pp. 23–32, 2013.
[40] D. L. Stern and D. J. Emlen, "The developmental basis for allometry in insects," *Development*, vol. 126, no. 6, pp. 1091–1101, 1999.
[41] C.-A. Darveau, P. W. Hochachka, K. C. Welch Jr., D. W. Roubik, and R. K. Suarez, "Allometric scaling of flight energetics in Panamanian orchid bees: A comparative phylogenetic approach," *J. Exp. Biol.*, vol. 208, no. 18, pp. 3581–3591, 2005.
[42] HySpex, "HySpex classic SWIR-384," Accessed: Jun. 7, 2021. [Online]. Available: https://www.hyspex.com/hyspex-products/hyspex-classic/hyspex-swir-384/
[43] MeadowlarkOptics, "Ultra broadband polarizer," Accessed: Jun. 7, 2021. [Online]. Available: https://www.meadowlark.com/ultrabroadband-polarizer/
[44] P. Debevec et al., "Estimating surface reflectance properties of a complex scene under captured natural illumination," *ACM Trans. Graph.*, vol. 1, pp. 1–11, Jan. 2004.
[45] F. Stanco, S. Battiato, and G. Gallo, *Digital Imaging for Cultural Heritage Preservation: Analysis, Restoration, and Reconstruction of Ancient Artworks*. Boca Raton, FL, USA: CRC, 2017.
[46] D. G. Stavenga, "Thin film and multilayer optics cause structural colors of many insects and birds," *Mater. Today: Proc.*, vol. 1, pp. 109–121, 2014.
[47] H. Yin et al., "Iridescence in the neck feathers of domestic pigeons," *Phys. Rev. E*, vol. 74, no. 5, 2006, Art. no. 051916.
[48] D. Raabe et al., "Microstructure and crystallographic texture of the chitin–protein network in the biological composite material of the exoskeleton of the lobster Homarus americanus," *Mater. Sci. Eng.: A*, vol. 421, no. 1, pp. 143–153, Apr. 2006.
[49] N. Katayama, J. K. Abbott, J. Kjærandsen, Y. Takahashi, and E. I. Svensson, "Sexual selection on wing interference patterns in Drosophila melanogaster," *Proc. Nat. Acad. Sci.*, vol. 111, no. 42, pp. 15144–15148, 2014.
[50] M. F. Hawkes et al., "Sexual selection drives the evolution of male wing interference patterns," *Proc. Roy. Soc. B: Biol. Sci.*, vol. 286, no. 1903, 2019, Art. no. 20182850.

Meng Li was born in Kunming, China in 1993. She received the M.Sc. degree in photonics in 2018 from Lund University, Lund, Sweden, where she is currently working toward the Ph.D. degree in biophotonics and remote sensing, with special focus on specular flashes from insect wings. In particular, using thin-film membrane thickness assessment as a tool to identify and monitor the diversity of insects.

Anna Runemark was born in Ronneby, Sweden in 1982. She received the M.Sc. degree in biology from Uppsala University, Uppsala, Sweden, and the Ph.D. degree in evolutionary animal ecology from Lund University, Lund, Sweden. She is currently working toward the Postdoctoral degree with the Centre for Ecological and Evolutionary Synthesis, University of Oslo, Oslo, Norway. She is also an Associate Senior Lecturer with the Department of Biology, Lund University.

Noélie Guilcher was born in Rennes, France in 1998. She received the M.Sc. degree in biological engineering from the Polytech Clermont-Ferrand School of Engineering, Aubière, France, in 2021. She completed Internship with Lund University, Lund, Sweden, in 2021.

Julio Hernandez was born in Mexico. He received the B.Sc. degree in physics from the National Autonomous University of Mexico, UNAM, Mexico City, Mexico and the M.Sc. degree in nanotechnology from the Chalmers University of Technology, Göteborg, Sweden. He is/was a Senior Research Scientist with Hyspex, Norsk Elektro Optikk AS in Oslo, Norway. He develops hyperspectral cameras and applications for remote sensing, defence and biomedical research in academia and industry.

Jadranka Rota was born in Zagreb, Croatia in 1976. She received the M.Sc. and Ph.D. degrees in entomology from the University of Connecticut, Storrs, CT, USA. She is/was a Postdoctoral Researcher with Smithsonian Institution, Washington, DC, USA, and Natural History Museum of Denmark, Copenhagen, Denmark. She is currently an insect Curator with Biological Museum, Department of Biology, Lund University, Lund, Sweden.

Mikkel Brydegaard was born in Copenhagen, Denmark in 1980. He received the M.Sc. degree in electrical Engineering in 2007, and the Ph.D. degree in atomic physics, biophotonics and remote sensing from Lund University, Lund, Sweden, in 2012. He is/was a Postdoctoral Research with Stellenbosch University, Stellenbosch, South Africa, and Norsk Elektro Optikk, Oslo, Norway. He was the recipient of the Inaba prize 2014, Docent 2016, a Senior Lecturer, in 2021 with Lund University, also ERC awardee 2018, and Co-Founder of the African Spectral Imaging Network and FaunaPhotonics, Denmark.